



MSUCL 908  
Ser 9418

Michigan State University

National Superconducting Cyclotron Laboratory

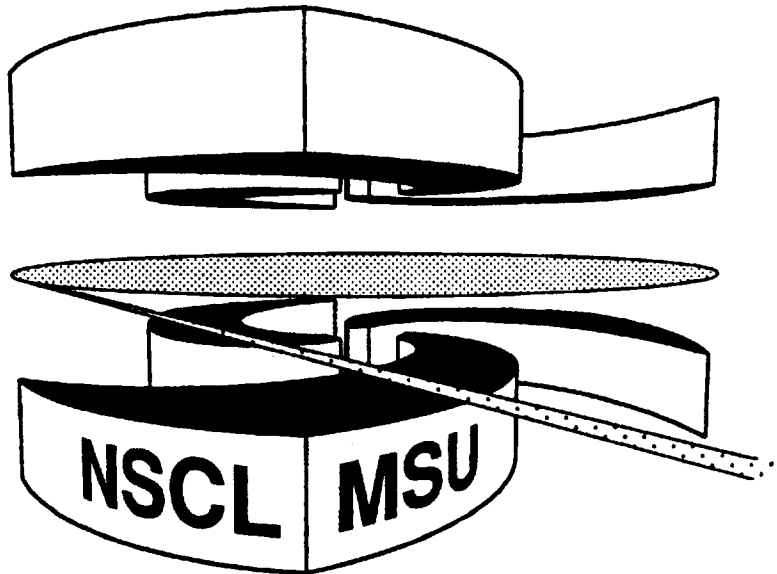
**AUTOCORRELATIONS AND  
INTERMEDIATE MASS FRAGMENT MULTIPLICITIES  
IN CENTRAL HEAVY-ION COLLISIONS.**

**W.J. LLOPE, J.A. CONRAD, C.M. MADER, G. PEILERT,  
W. BAUER, D. CRAIG, E. GUALTIERI, S. HANNUSCHKE,  
R.A. LACEY, J. LAURET, T. LI, A. NADASEN, E. NORBECK,  
R. PAK, N.T.B. STONE, A.M. VANDER MOLEN,  
G.D. WESTFALL, J. YEE, AND S.J. YENNELLO.**

CERN LIBRARIES, GENEVA



P00022413



MSUCL-908

APRIL 1994

# Autocorrelations and intermediate mass fragment multiplicities in central heavy-ion collisions.

W.J. Llope<sup>1,§</sup>, J.A. Conrad<sup>1,\*</sup>, C.M. Mader<sup>1,†</sup>, G. Peilert<sup>2</sup>  
W. Bauer<sup>1</sup>, D. Craig<sup>1</sup>, E. Gualtieri<sup>1</sup>, S. Hannuschke<sup>1</sup>, R.A. Lacey<sup>3</sup>,  
J. Lauret<sup>3</sup>, T. Li<sup>1</sup>, A. Nadasen<sup>4</sup>, E. Norbeck<sup>6</sup>, R. Pak<sup>1</sup>, N.T.B. Stone<sup>1</sup>,  
A.M. Vander Molen<sup>1</sup>, G.D. Westfall<sup>1</sup>, J. Yee<sup>1</sup>, and S.J. Yennello<sup>3</sup>.

1. National Superconducting Cyclotron Laboratory, Michigan State University, E. Lansing, MI 48824

2. Lawrence Livermore National Laboratory, Livermore, CA 94550

3. Department of Chemistry, State University of New York - Stony Brook, Stony Brook, NY 11794

4. Department of Physics, U. of Michigan - Dearborn, Dearborn, MI 48128

5. Cyclotron Institute, Texas A&M University, College Station, TX 77843

6. Department of Physics and Astronomy, U. of Iowa, Iowa City, IA 52242

April 17, 1994

## Abstract

The average multiplicities of intermediate mass fragments (IMFs) for central heavy-ion collisions in the (nearly) symmetric entrance channels  $^{20}\text{Ne}+^{27}\text{Al}$ ,  $^{40}\text{Ar}+^{45}\text{Sc}$ ,  $^{84}\text{Kr}+^{93}\text{Nb}$ , and  $^{129}\text{Xe}+^{139}\text{La}$ , are systematically studied over a wide range of intermediate beam energies. Cuts on experimental variables commonly assumed to be correlated with the impact parameter are used to select the most central collisions. The results for six different centrality variables are compared, and the extent to which measurements of the multiplicities of IMFs in small impact parameter collisions are affected by the variable used to select the central events is discussed. The two centrality observables that are the least autocorrelated with the number of intermediate mass fragments are identified. These variables are used to select the most central collisions. The entrance channel mass and beam energy dependence of the experimental IMF multiplicities are presented and compared to a variety of model predictions. The models picturing the disassembly as a sequential binary process always underpredict the experimental IMF multiplicities. A generally more accurate reproduction of these multiplicities is provided by several similar chemical equilibrium models commonly assumed to be the theoretical description of multifragmentation.

# 1 INTRODUCTION

Perhaps the most direct study of multifragment final states following intermediate energy heavy-ion collisions involves the experimental measurement of the average number of intermediate mass fragments (IMFs, for which  $3 \leq Z \lesssim 20$ ) emitted in such reactions. A number of physical processes governing the disassembly of excited nuclei can result in the emission of such fragments (see the recent review by Moretto and Wozniak [1]), and many model code event generators embodying these processes are available. One general class of these models is fundamentally “sequential binary”, i.e. these describe the disassembly as a series of two-body decay steps, each involving (a)symmetric fission or statistical evaporation. An alternative description is provided by several similar “multifragmentation” models, which assume chemical and thermal equilibrium has been obtained in an expanded spherical freeze-out volume of prescribed size. Previously reported comparisons of the results obtained from models in these two general classes imply that larger multiplicities of IMFs are obtained from the multifragmentation models, as compared to the sequential binary models run with the same set of input parameters [2]. This observation was, however, subsequently contested [3]. Systematic experimental measurements of IMF emission from nuclear systems covering a wide range of mass and excitation are required, allowing the confrontation of all the various theoretical predictions with experimental results.

In this paper, the average multiplicities of IMFs in central  $^{20}\text{Ne}+^{27}\text{Al}$ ,  $^{40}\text{Ar}+^{45}\text{Sc}$ ,  $^{84}\text{Kr}+^{93}\text{Nb}$ , and  $^{129}\text{Xe}+^{139}\text{La}$  reactions will be presented. Each entrance channel was measured using the MSU  $4\pi$  Array [4] at many beam energies ranging from 15 to 135 MeV/nucleon. The average IMF multiplicities in the central experimental collisions will be compared to those obtained from events generated using a variety of models. This generation was done in both hybrid and dynamic approaches, and the events were filtered through a detailed software replica of the experimental apparatus. The accuracy by which the filtered model codes reproduce the multiplicities of IMFs in the central experimental collisions will be described.

Six experimental observables (“centrality variables”) are assumed to be correlated with the impact parameter, and maximal values of each centrality variable are expected from the most central events. Cuts will be placed on these variables, allowing the experimental selection of the central nucleus-nucleus collisions in these data. It is noted, however, that the particular choice of the variable upon which a selection of central collisions is performed may affect the measurement of the average multiplicities of IMFs due to constraints imposed on the reactions by charge or mass conservation laws.


The degree of “autocorrelation” between each of the six centrality variables and the average multiplicities of intermediate mass fragments in these data must therefore be inferred. Such autocorrelations are an important source of bias for the study of any experimental observable following a selection of central collisions. We assume that autocorrelations are reflected in the variances of the observable in different samples of small impact parameter events selected by cuts on many different centrality variables. The centrality cuts that artificially enhance or suppress the average multiplicities of IMFs in the selected central events will be identified. Two dimensional cuts will be placed on the two centrality variables that are the least autocorrelated with the multiplicities of IMFs for an internally unbiased measurement of this observable in the most central collisions. This will allow the comparison

of the average IMF multiplicities obtained from the experimental and model generated events, and inferences concerning the validity of each model for the description of these multiplicities.

This paper is organized as follows. Section 2 describes the investigation of the autocorrelations between six different centrality variables and the observed multiplicities of IMFs. The centrality variables that are the least autocorrelated with the IMF multiplicities,  $N_{IMF}$ , in small impact parameter collisions are defined. The entrance channel mass and beam energy dependence of  $\langle N_{IMF} \rangle$  in the central events selected using these non-autocorrelating variables are presented. The comparison of these experimental IMF multiplicities with those obtained from a number of filtered model codes are described in Section 3. The summary and conclusions are presented in Section 4.

## 2 AUTOCORRELATIONS AND THE SELECTION OF CENTRAL COLLISIONS

In central heavy-ion reactions there are large probabilities for the formation of highly excited nuclear systems that contain most of the nucleons in the entrance channel. The excitation energies in these systems are monotonic functions of the beam energy. Such events can be selected offline via software cuts on experimental variables that are correlated with the impact parameter. The variable upon which a centrality cut is made must be tightly correlated with the impact parameter, and negligibly correlated with the experimental observable in all ways except that via the impact parameter. A significant correlation between an experimental observable and the centrality variable (beyond that due to the impact parameter) can be caused by charge, mass, or momentum conservation laws. Such ‘‘autocorrelations’’ may artificially enhance or suppress the values of the experimental observable in the events selected by perfunctory centrality cuts. In this Section, the degree of autocorrelation between six different centrality variables and the average multiplicities of IMFs in a comprehensive set of small impact parameter reactions will be investigated.

The experimental data were collected with the Michigan State University  $4\pi$  Array  at the National Superconducting Cyclotron Laboratory (NSCL) using beams extracted from the K1200 cyclotron. Four symmetric entrance channels were systematically studied over a wide range of intermediate beam energies. The reactions include  $^{20}\text{Ne}+^{27}\text{Al}$  at 55, 75, 95, 105, 115, 125, 135 MeV/nucleon,  $^{40}\text{Ar}+^{45}\text{Sc}$  at 15, 25, 35, 45, 65, 75, 85, 105, 115 MeV/nucleon,  $^{84}\text{Kr}+^{93}\text{Nb}$  at 35, 45, 55, 65, 75 MeV/nucleon, and  $^{129}\text{Xe}+^{139}\text{La}$  at 25, 35, 45, 50, 55, 60 MeV/nucleon. Detailed descriptions of the apparatus and the data collection can be found in Refs. [4, 5].

There is an intrinsic width to experimental observables in perfectly central collisions that is caused by the stochastic nature of the evolution of the excited nuclear systems formed in these collisions. Additional experimental contributions to this width result from any dependence of the experimental acceptance on the orientation of these excited systems in the laboratory, and from any inefficiencies in the selection of the most central collisions. These experimental contributions can be understood via the study of the effect that a software replica of the experimental apparatus has on events generated by model codes at specific impact parameters (see Section 3). In principle, the intrinsic width carries important physical information concerning fluctuations during the reactions. The measured width can, after the treatment of the experimental contributions, be defined as the intrinsic width, unless there are non-negligible autocorrelations between the observable  $O$  and the experimental variable

used to select the central events.

It is assumed that the variance,  $\sigma_O^2 = \langle O^2 \rangle - \langle O \rangle^2$ , of an observable,  $O$ , in a sample of selected events is suppressed if a significant autocorrelation exists, and is equal to the intrinsic variance or width (modified by experimental considerations) otherwise. The importance of such autocorrelations during the use of a particular centrality variable can thus be inferred by the comparison of the variance of the observable following the selection of central events using many different centrality variables. The cut(s) leading to the largest variances,  $\sigma_O^2$ , in the selected events are assumed to be the least autocorrelated with  $O$ . Two classes of autocorrelations between a centrality cut and an experimental observable can be defined based on the effects that such autocorrelations have on the normalized variance,  $\sigma_O^2/\langle O \rangle$ , in the selected events. Centrality cuts which result in a suppressed variance and a suppressed(enhanced) normalized variance will be referred to as positive(negative) autocorrelators, as they artificially enhance(suppress)  $\langle O \rangle$ .

The following variables are assumed to be correlated with the impact parameter: (i) the number of charged particles ( $N_{chgd}$ ) detected in each event, (ii) the total charge detected in a software gate centered at mid-rapidity ( $Z_{MR}$ ), (iii) the total transverse kinetic energy ( $KE_T$ ), (iv) the number of detected hydrogen isotopes ( $N_H$ ), (v) the total detected charge ( $Z_{det}$ ), and (vi) the total charge of hydrogen and helium isotopes particles ( $Z_{LCP}$ ). The variables  $Z_{MR}$  and  $KE_T$  are defined as in Ref. [6]. Separate samples of events are formed by placing thresholds on the impact parameter inclusive spectra of each of these variables which allow the most central  $\sim 10\%$  of the events. For all of the centrality variables that are integer quantities, i.e. all but  $KE_T$ , it is not always possible to locate a threshold such that exactly 10% of the minimum bias events are selected. The threshold was thus defined for each centrality variable and reaction as the lowest bin for which  $\leq 10\%$  of the impact parameter inclusive events are in or above this bin. According to approximate geometrical arguments, thresholds allowing 10% of the impact parameter inclusive events allow average impact parameters  $\langle b \rangle \sim 0.31b_{max}$ . The quantity  $b_{max}$  is the largest impact parameter satisfying the minimum bias trigger used to collect these data, which required two or more charged particle hits in the MSU  $4\pi$  Array. The quantity  $b_{max}$  is typically assumed to equal  $[R_P + R_T]$ , where  $R_P(R_T)$  is the radius of the projectile(target) nucleus.

In Figures 1 and 2, the means (upper frames), variances (middle frames), and normalized variances (lower frames) of the  $N_{IMF}$  distributions are presented versus the beam energy in the six samples of selected small impact parameter events. The  $^{20}\text{Ne}+^{27}\text{Al}$  and  $^{40}\text{Ar}+^{45}\text{Sc}$  entrance channels are shown in Figure 1, while the  $^{84}\text{Kr}+^{93}\text{Nb}$  and  $^{129}\text{Xe}+^{139}\text{La}$  reactions are shown in Figure 2. The statistical errors in these Figures are smaller than the size of the points, while the systematic errors are discussed in Section 3.

For all four entrance channels, the beam energy dependence of the IMF multiplicity observables is generally not affected by the particular choice of the variable used to select the small impact parameter events. In the  $^{20}\text{Ne}+^{27}\text{Al}$  reactions ( $E_{proj} \geq 55$  MeV/nucleon), the values of  $\langle N_{IMF} \rangle$  decrease with increasing beam energies. In the  $^{40}\text{Ar}+^{45}\text{Sc}$  reactions, the experimental values of  $\langle N_{IMF} \rangle$  increase with increasing beam energies up to about 35 MeV/nucleon, and then fall off slowly for larger beam energies. For both of the heavier systems,  $^{84}\text{Kr}+^{93}\text{Nb}$  ( $E_{proj} \leq 75$  MeV/nucleon) and  $^{129}\text{Xe}+^{139}\text{La}$  ( $E_{proj} \leq 60$  MeV/nucleon), the values of  $\langle N_{IMF} \rangle$  increase with increasing beam energies.

In Figures 1 and 2, the IMF multiplicity observables in the events selected by the six

different centrality cuts generally form three distinct groups independent of the beam energy. Centrality cuts on the variables  $Z_{MR}$  and  $Z_{det}$  result in  $N_{IMF}$  distributions with relatively small variances and small normalized variances, while cuts on the variables  $N_H$  and  $Z_{LCP}$  result in relatively small variances and relatively large reduced variances. The events selected by the cuts on the variables  $N_{chgd}$  and  $KE_T$  have the relatively largest variances and intermediate reduced variances. Some exceptions to these trends in  $\sigma^2(N_{IMF})$  are noted. At the highest beam energies in the  $^{20}\text{Ne}+^{27}\text{Al}$  entrance channel, the variances following the  $Z_{MR}$  and  $Z_{det}$  cuts exceed those following the  $N_{chgd}$  and  $KE_T$  cuts. In the two heavier systems (Figure 2), the variances from the  $N_H$  and  $Z_{LCP}$  cuts are similar to those from the  $N_{chgd}$  and  $KE_T$  cuts (and relatively large). However, for all of the reactions, the normalized variances are always ordered in the same way.

The formation of these groups is generally independent of the beam energy and the entrance channel mass, which implies that the grouping is the consequence of an internal effect rather than physical one. The formation of these groups is a reflection of autocorrelations between some of these centrality variables and  $N_{IMF}$ . The centrality variables  $N_H$  and  $Z_{LCP}$  apparently suppress  $\langle N_{IMF} \rangle$  (and  $\sigma^2$ ) and are thus defined to be negative autocorrelators, while the variables  $Z_{MR}$  and  $Z_{det}$  artificially enhance  $\langle N_{IMF} \rangle$  and are labelled positive autocorrelators. Given the dramatic distortions to IMF multiplicity observables seen in Figures 1 and 2 that result from centrality cuts on variables that autocorrelate with  $N_{IMF}$ , the only acceptable study of these observables in the central collisions in these data must involve cuts on  $N_{chgd}$  and/or  $KE_T$ . Figures 1 and 2 imply that the negative autocorrelation between the light particle multiplicity variables and  $N_{IMF}$  is somewhat stronger than the positive autocorrelation between  $N_{IMF}$  and the variables  $Z_{MR}$  and  $Z_{det}$ .

To limit the selection of larger impact parameter events with significant topological fluctuations, a two-dimensional cut is placed on the centrality variables  $N_{chgd}$  and  $KE_T$  for all of the systems and beam energies. Only the events that fall above the thresholds located as described above (each allowing  $\lesssim 10\%$  of the events) for both of these variables are selected. This results in the selection of  $\sim 4\text{--}7\%$  of the events, which have average impact parameters  $\langle b \rangle \sim 0.20 - 0.26 b_{max}$  geometrically.

The mean multiplicities of IMFs in the events selected by these two-dimensional cuts are shown for all of the entrance channels and beam energies in Figure 3 as the solid squares. The average IMF multiplicities in the events selected by the two one-dimensional cuts on  $N_{chgd}$  (open circles) and  $KE_T$  (open triangles) are also shown. The events selected by the two-dimensional cut exhibit larger values of  $\langle N_{IMF} \rangle$  as compared to those following either of the one-dimensional cuts. For increasing beam energies, the values of  $\langle N_{IMF} \rangle$  decrease in the central  $^{20}\text{Ne}+^{27}\text{Al}$  reactions ( $E_{proj} \geq 55$  MeV/nucleon), rise then fall in the central  $^{40}\text{Ar}+^{45}\text{Sc}$  reactions, and increase in the central  $^{84}\text{Kr}+^{93}\text{Nb}$  ( $E_{proj} \leq 75$  MeV/nucleon) and  $^{129}\text{Xe}+^{139}\text{La}$  reactions ( $E_{proj} \leq 60$  MeV/nucleon). The average IMF multiplicities range from  $\sim 0.4$  for the highest energy  $^{20}\text{Ne}+^{27}\text{Al}$  reactions to  $\sim 5.5$  for the highest energy  $^{129}\text{Xe}+^{139}\text{La}$  reactions.

The variances,  $\sigma^2(N_{IMF})$ , in these same samples of small impact parameter events are shown in Figure 4. The variances from the two-dimensional  $\sim 10\%$  cuts (solid squares) are larger than the variances from the two one-dimensional cuts (open circles and triangles) in the  $^{20}\text{Ne}+^{27}\text{Al}$  and  $^{40}\text{Ar}+^{45}\text{Sc}$  reactions, and they are similar to or between the values from the two one-dimensional cuts in the  $^{84}\text{Kr}+^{93}\text{Nb}$  and  $^{129}\text{Xe}+^{139}\text{La}$  reactions. Also shown in

this Figure are the  $N_{IMF}$  variances from stricter two-dimensional  $\sim 2\%$  cuts on  $N_{chgd}$  and  $KE_T$  (solid triangles). It is important to note that the  $N_{IMF}$  variances from these stricter two-dimensional  $\sim 2\%$  cuts are always larger than those from the two-dimensional  $\sim 10\%$  cuts (solid squares). This corroborates the statement that the variables  $N_{chgd}$  and  $KE_T$  do not autocorrelate with  $N_{IMF}$  in these data, as stricter cuts must magnify the importance of the conservation law that drives the autocorrelation.

The average multiplicities of IMFs are depicted versus the total charged particle multiplicity in Figure 5. For all of the available entrance channels and beam energies, the largest average multiplicities of IMFs are found in the events with the largest total charged particle multiplicities. In this Figure, the solid points for each system and beam energy are those above the  $\sim 10\%$  cuts on  $N_{chgd}$  alone described above. A roughly universal dependence of  $\langle N_{IMF} \rangle$  on  $N_{chgd}$  is noted for the more peripheral collisions (open points).

It is important to investigate the effects that the inefficiencies in the experimental measurement have on the average IMF multiplicities shown in Figures 3 and 5. This is performed via the generation of events by model codes, and the filtering of these events by a software replica of the MSU  $4\pi$  Array. A number of different model codes were used to allow the study of the values of  $\langle N_{IMF} \rangle$  predicted in the sequential binary and multifragmentation approaches, and the evaluation of the accuracy by which these approaches reproduce the experimental values of  $\langle N_{IMF} \rangle$ . Such a study is described in the next Section.

### 3 COMPARISONS TO MODEL PREDICTIONS

Many different physical mechanisms that may govern the disassembly of excited nuclei can lead to the emission of intermediate mass fragments [1]. In this Section, we describe the results obtained from models that embody assumptions from a variety of theoretical approaches for describing central intermediate energy heavy-ion collisions. The purpose of these calculations is twofold. First, the different calculations are performed as consistently as possible, so that the average IMF multiplicities from the different models can be directly compared. Several investigations of this sort have been published [2], and these imply that larger average IMF multiplicities are obtained from multifragmentation models compared to consistently run sequential binary calculations. However, some disagreement with this claim was discussed in Ref. [3], following a study of calculated massive fragment ( $Z \geq 5$ ) multiplicities. Second, under the assumption that the chosen input parameters to the different calculations are reasonably realistic, the average IMF multiplicities from the models can be directly compared to the experimentally measured values described in the previous Section.

The event generation was performed in both dynamic and hybrid approaches. The “afterburners” used in the hybrid event generation were the Berlin [7] and Copenhagen [8] multifragmentation codes, as well as the sequential binary code Gemini [9]. The Berlin and Copenhagen codes are similar in philosophy, and assume that the system comes to thermal and chemical equilibrium within an expanded volume that is spherical and of prescribed radius. The various fragmentation channels occur with probabilities obtained from the channels’ entropy, which is obtained using a finite temperature liquid drop model. The code Gemini pictures the disassembly as a sequence of binary fissions, using Bohr-Wheeler fission widths and conditional barriers from a shape adjusted two-spheroid finite range calculation, followed by evaporation according to a Hauser-Feshbach description.

All of these were run with the default parameters with the exception of the charge, mass, and excitation energy in the composite system, which was extracted from Boltzmann-Uehling-Uehlenbeck (BUU) calculations [10] in the same manner as described in Ref. [11]. These calculations describe the evolution of the one-body phase space distribution following the Boltzmann equation, including approximately Pauli-blocked scattering, via ensemble averaging. A soft equation of state was assumed, and the calculations were terminated when the radial density profile of the composite system most closely resembled that of a ground state nucleus [12]. The excitation energy of the excited system at rest in the center of momentum (CM) frame is then calculated as the total energy of this system minus a liquid-drop energy for a ground state nucleus with the same charge and mass. The calculations were performed at an impact parameter of  $b = 0.20[R_P + R_T]$ .

The excitation energies predicted by the BUU calculations for the selected events in each reaction are shown in Figure 6. A recent analysis [13] has noted differences in the IMF multiplicities obtained when an afterburner code is supplied with a single average excitation energy or excitation energies separately calculated for each event. However, given the large number of different reactions and afterburner model codes studied here, a dynamic calculation of the afterburner input parameters for each generated event is computationally prohibitive. The mass and charge of the composite predicted by the BUU calculations is generally  $\sim 90\%$  of the total entrance channel mass and charge. In the present BUU hybrid event generation, the remaining particles are thermally emitted from projectile and target-like sources, using reasonable assumptions for the velocities, temperatures, and emitted charge distributions of these sources for each reaction.

The Berlin and Gemini codes also require a cut-off angular momentum. For the BUU+Berlin calculations, the values used were  $36\hbar$ ,  $62\hbar$ ,  $80\hbar$ , and  $70\hbar$  for the central  $^{20}\text{Ne}+^{27}\text{Al}$ ,  $^{40}\text{Ar}+^{45}\text{Sc}$ ,  $^{84}\text{Kr}+^{93}\text{Nb}$ , and  $^{129}\text{Xe}+^{139}\text{La}$  reactions, respectively. The angular momenta of the excited systems in the selected experimental events may very well exceed the values assumed above, presumably leading to decays involving a fast fission. The BUU+Gemini calculations were therefore also performed using cut-off angular momenta both well above and below the values listed above.

Complete events from a hybrid model involving a Quantum Molecular Dynamics (QMD) [14] initial stage and Copenhagen disassembly were also produced for  $^{36}\text{Ar}+^{45}\text{Sc}$  reactions for impact parameters  $b \leq 4$  fm. The QMD calculations describe the evolution of a system of gaussian wave packets (nucleons) that move under the influence of mutual two and three body forces and scatter in approximate respect of the Pauli principle. Although hybrid in the sense that the reaction is described in two steps, the QMD+Copenhagen calculations are dynamic in the sense that the impact parameter for each calculated event is known. Another model with this feature is the code Freesco [15], which does not require a separate BUU or QMD description of the initial stage of the reaction. This model divides the colliding nuclei into two spectator sources and a participant source, which share energy and angular momenta, according to the impact parameter. The decay of these sources is described by a microcanonical calculation similar in philosophy to those in the Berlin and Copenhagen models, including a simplified description of the evaporation.

A software reproduction of the experimental apparatus is used to filter the events obtained in all of the approaches listed above. This code contains a detailed treatment of the geometry of the device including all inactive regions, the run-dependent particle kinetic



energy thresholds for all measurable particles, the particle kinetic energy loss in the target and associated support assembly, and multiple particle hits in individual detector elements. The calculation of the result of a multiple hit involves the same particle charge and energy templates used to calibrate all of the raw experimental data. Following the passage through the filter code, the generated events appear as they would experimentally, up to a conservatively assumed systematic uncertainty of  $\sim 30\%$  in the values of  $\langle N_{IMF} \rangle$  from the filtered simulations.

The multiplicities of IMFs can also be calculated using model codes which do not generate samples of complete events. Examples of these are the statistical evaporation code of Ref. [16], and the Quantum Statistical Model [17]. The model of Ref. [16] follows the ensemble averaged evolution of a system that statistically emits particles in a sequence of two-body decay steps. This model thus provides a description of sequential binary disassembly that is alternative to the (fission-evaporation) Gemini code. The Fermi energy used as input in this model was 25 MeV for the central  $^{20}\text{Ne}+^{27}\text{Al}$  and  $^{40}\text{Ar}+^{45}\text{Sc}$  reactions, and 30 MeV for the central  $^{84}\text{Kr}+^{93}\text{Nb}$  and  $^{129}\text{Xe}+^{139}\text{La}$  reactions [18]. However, as complete events are not provided by this code, the experimental inefficiencies for the measurement of  $N_{IMF}$  can only be imposed approximately. This is done by extracting the average efficiency for detecting IMFs from each of the filtered event-generating models listed above for all entrance channels and beam energies. These efficiencies are generally between 50% and 80%, depending on the reaction and the approach used to generate the complete events. For each reaction separately, the minimum and maximum IMF measurement efficiencies obtained from the different model calculations are multiplied by the IMF multiplicities obtained from the statistical evaporation code. This defines a range of IMF multiplicities for each reaction presumed to contain the predictions of the statistical evaporation code including the effects of the experimental inefficiencies.

The average IMF multiplicities in the central  $^{20}\text{Ne}+^{27}\text{Al}$ ,  $^{40}\text{Ar}+^{45}\text{Sc}$ ,  $^{84}\text{Kr}+^{93}\text{Nb}$ , and  $^{129}\text{Xe}+^{139}\text{La}$  reactions are shown in Figures 7-10, respectively. The experimental values from the two-dimensional  $\sim 10\%$  central cut (on  $N_{chgd}$  and  $KE_T$ ) are shown by the solid points, while the values from the two one-dimensional  $\sim 10\%$  cuts (on  $N_{chgd}$  and  $KE_T$ , separately) are given by the open points. The lines in the upper frame in each of these Figures are the values predicted by the filtered BUU+Berlin (solid), and BUU+Copenhagen (dashed) calculations. In Figure 8 only, the upper frame also includes the predictions of the filtered QMD+Copenhagen calculations, which were run under the same assumptions used to generate the BUU+Berlin and BUU+Copenhagen events. The lines in the middle frames depict the predictions of the filtered Freesco code, which was run for maximum impact parameters of  $0.01(R_P + R_T)$  (solid),  $0.20(R_P + R_T)$  (dashed), and  $0.40(R_P + R_T)$  (dot-dashed). The lower frames include the predictions of the filtered BUU+Gemini calculations, which were performed for maximum angular momenta of  $10\hbar$  (solid),  $70\hbar$  (dashed), and  $200\hbar$  (dot-dashed).

The experimental IMF multiplicities in the central  $^{20}\text{Ne}+^{27}\text{Al}$  reactions (Figure 7) at beam energies near and above 100 MeV/nucleon agree with the BUU+Berlin, BUU+Copenhagen, and Freesco calculations. For lower beam energies in this system, however, the BUU+Berlin and BUU+Copenhagen calculations overestimate the experimental values. The calculated IMF multiplicities increase slowly with decreasing maximum impact parameters in the filtered Freesco calculations. The IMF multiplicities obtained from the filtered

BUU+Gemini events increase with increases in the maximum angular momentum allowed in the calculation. However, even for maximum angular momenta well in excess of that which can be supported by the systems expected to be formed in the central  $^{20}\text{Ne}+^{27}\text{Al}$  collisions, the BUU+Gemini IMF multiplicities underpredict the experimental values.

The filtered BUU+Berlin and BUU+Copenhagen calculations predict (Figure 8) a sharp rise in the IMF multiplicities for the central  $^{40}\text{Ar}+^{45}\text{Sc}$  reactions near beam energies of 40 MeV/nucleon. The experimental IMF multiplicities for these reactions exhibit such a rise for beam energies somewhere between 25 and 35 MeV/nucleon. These two approaches significantly underestimate the experimental IMF multiplicities below 35 MeV/nucleon, and reasonably reproduce the experimental values for larger beam energies. The QMD+Copenhagen calculations predict about a factor of two fewer IMFs than observed experimentally for all beam energies. These QMD+Copenhagen predictions are quite insensitive to the stiffness of the equation of state used in the QMD phase, or the radius of the critical freeze-out volume assumed in the subsequent Copenhagen calculation, for all of the central  $^{40}\text{Ar}+^{45}\text{Sc}$  reactions. The filtered Freesco calculations predict a sharp rise in the IMF multiplicities near 35-45 MeV/nucleon, depending on the impact parameter region allowed in the calculation. These calculations generally reproduce the experimental results at beam energies above  $\sim 45$  MeV/nucleon if  $b_{max} \lesssim 0.2(R_P + R_T)$ , and again lead to significant underestimates at lower beam energies. The BUU+Gemini calculations significantly underestimate the experimental IMF multiplicities for all three values the maximum angular momenta allowed in these calculations and for all beam energies.

The conclusions drawn for the central  $^{84}\text{Kr}+^{93}\text{Nb}$  (Figure 9) and  $^{129}\text{Xe}+^{139}\text{La}$  (Figure 10) reactions are generally similar to those drawn from the central  $^{40}\text{Ar}+^{45}\text{Sc}$  reactions. The BUU+Berlin and BUU+Copenhagen calculations underestimate the experimental IMF multiplicities at the lowest available beam energies, and provide a better reproduction of the experimental values at larger beam energies. The filtered Freesco calculations give a reasonable description on the IMF multiplicities for all of the available beam energies in these entrance channels. The BUU+Gemini calculations again lead to underestimates for all beam energies and maximum angular momenta allowed in the calculation.

The comparison of the experimental IMF multiplicities and those from the statistical evaporation code of Ref. [16], following the approximate treatment of the experimental inefficiencies, is shown in Figure 11. For all of the reactions studied in this analysis, these calculations significantly underpredict the observed IMF multiplicities. This underprediction is similar to that from the filtered BUU+Gemini calculations.

## 4 SUMMARY AND CONCLUSIONS

This analysis has investigated the average multiplicities of intermediate mass fragments emitted following central heavy-ion reactions in four near symmetric entrance channels, each at many intermediate beam energies. The average IMF multiplicities were shown to be significantly affected by possible autocorrelations with the variables upon which the impact parameter of each event was inferred. Six different centrality variables were compared, and those variables that are not autocorrelated with the IMF multiplicities for small impact parameter collisions were identified. These variables were the total charged particle multiplicity and the total transverse kinetic energy. Experimental observables other than the IMF

multiplicities were not studied in this paper, but general methods allowing the identification of autocorrelating centrality cuts for any experimental observable were described.

Predictions for the average multiplicities of IMFs in small impact parameter collisions were obtained from a variety of theoretical model codes. These predictions were filtered through a detailed software replica of the experimental apparatus. The average IMF multiplicities obtained from the various sequential binary models were always less than those obtained from the multifragmentation models. The experimental results were generally more accurately described by the multifragmentation models, with notable exceptions from some of these models for beam energies near and below  $\sim 35$  MeV/nucleon.

### ACKNOWLEDGEMENTS

A portion of this work comprises the Masters Thesis of J.A. Conrad (Michigan State University, 1993, unpublished). We thank W.G. Lynch for providing the source code for the model of Ref. [16]. This work is supported by the U.S. National Science Foundation under the Grants No. PHY 89-13815 and No. PHY 92-14992.

---

§ Electronic mail address: llope@nscl.nsl.msue.edu.

\* Present address: Hughes STX, Goddard Space Flight Center, Code 921, Greenbelt, MD 20771.

† Present address: Department of Physics, Hope College, Holland, MI 49423.

### References

- [1] L.G. Moretto and G.J. Wozniak, *Ann. Rev. Nucl. Part. Sci.* (May, 1993).
- [2] A.S. Botvina, A.S. Iljinov, and I.N. Mishustin, *Phys. Lett. B* **205**, 421 (1988);  
H.Y. Han, K.X. Jing, E. Plagnol, D.R. Bowman, R.J. Charity, L. Vinet, G.J. Wozniak, and L.G. Moretto, *Nucl. Phys.* **A492**, 138 (1989);  
J. Hubele, P. Kreuzt, V. Lindenstruth, J.C. Adloff, M. Begemann-Blaich, P. Bouissou, G. Imme, I. Iori, G.J. Kunde, S. Leray, Z. Liu, U. Lynen, R.J. Meijer, U. Milkau, A. Moroni, W.F.J. Müller, C. Ngô, C.A. Ogilvie, J. Pochodzalla, G. Raciti, G. Rudolf, H. Sann, A. Schüttauf, W. Seidel, L. Stuttge, W. Trautmann, A. Tucholski, R. Heck, A.R. DeAngelis, D.H.E. Gross, H.R. Jaqaman, H.W. Barz, H. Schulz, W.A. Friedman, and R.J. Charity, *Phys. Rev. C* **46**, R1577 (1992).
- [3] R. Donangelo, J.A. López, and J. Randrup, *Phys. Rev. C* **48**, 465 (1993).
- [4] G.D. Westfall, J.E. Yurkon, J. Van Der Plicht, Z.M. Koenig, B.V. Jacak, R. Fox, G.M. Crawley, M.R. Maier, B.E. Hasselquist, R.S. Tickle, and D. Horn, *Nucl. Inst. and Methods* **A238**, 347 (1985).

- [5] G.D. Westfall, W. Bauer, D. Craig, M. Cronqvist, E. Gualtieri, S. Hannuschke, D. Klakow, T. Li, T. Reposeur, A.M. Vander Molen, W.K. Wilson, J.S. Winfield, J. Yee, S.J. Yennello, R.A. Lacey, A. Elmaani, J. Lauret, A. Nadasen, and E. Norbeck, *Phys. Rev. Lett.* **71**, 1986 (1993);
- E. Bauge, A. Elmaani, R.A. Lacey, J. Lauret, N.N. Ajitanand, D. Craig, M. Cronqvist, E. Gualtieri, S. Hannuschke, T. Li, W.J. Llope, T. Reposeur, A.M. Vander Molen, G.D. Westfall, J.S. Winfield, J. Yee, S.J. Yennello, A. Nadasen, and E. Norbeck, *Phys. Rev. Lett.* **70**, 3705 (1993);
- T. Li, W. Bauer, D. Craig, M. Cronqvist, E. Gualtieri, S. Hannuschke, R.A. Lacey, W.J. Llope, T. Reposeur, A.M. Vander Molen, G.D. Westfall, W.K. Wilson, J.S. Winfield, J. Yee, S.J. Yennello, A. Nadasen, R.S. Tickle, E. Norbeck, *Phys. Rev. Lett.* **70**, 1924 (1993);
- R.A. Lacey, A. Elmaani, J. Lauret, T. Li, W. Bauer, D. Craig, M. Cronqvist, E. Gualtieri, S. Hannuschke, T. Reposeur, A.M. Vander Molen, G.D. Westfall, W.K. Wilson, J.S. Winfield, J. Yee, S.J. Yennello, A. Nadasen, R.S. Tickle, and E. Norbeck, *Phys. Rev. Lett.* **70**, 1224 (1993).
- [6] L. Phair, D.R. Bowman, C.K. Gelbke, W.G. Gong, Y.D. Kim, M.A. Lisa, W.G. Lynch, G.F. Peaslee, R.T. de Souza, M.B. Tsang, and F. Zhu, *Nucl. Phys.* **A548**, 489 (1992).
- [7] D.H.E. Gross, *Prog. Part. Nucl. Phys.* **30**, 155 (1993), and references therein.
- [8] J.P. Bondorf, R. Donangelo, I.N. Mushustin, C.J. Pethick, H. Schulz, and K. Sneppen, *Nucl. Phys.* **A443**, 321 (1985);
- J.P. Bondorf, R. Donangelo, I.N. Mushustin, and H. Schulz, *Nucl. Phys.* **A444**, 460 (1985).
- [9] R.J. Charity, M.A. McMahan, G.J. Wozniak, R.J. McDonald, L.G. Moretto, D.G. Sarantites, L.G. Sobotka, G. Guarino, A. Pantaleo, L. Fiore, A. Gobbi, and K.D. Hildenbrand, *Nucl. Phys.* **A483**, 371 (1988).
- [10] W. Bauer, G.F. Bertsch, W. Cassing, and U. Mosel, *Phys. Rev. C* **34**, 2127 (1986);
- W. Bauer, *Phys. Rev. Lett.* **61**, 2534 (1988).
- [11] D.R. Bowman, C.M. Mader, G.F. Peaslee, W. Bauer, N. Carlin, R.T. de Souza, C.K. Gelbke, W.G. Gong, Y.D. Kim, M.A. Lisa, W.G. Lynch, L. Phair, M.B. Tsang, C. Williams, N. Colonna, K. Hanold, M.A. McMahan, G.J. Wozniak, L.G. Moretto, and W.A. Friedman, *Phys. Rev. C* **46**, 1834 (1992).
- [12] C.M. Mader, Ph.D. Thesis, Michigan State University, 1993 (unpublished).
- [13] K. Kwiatkowski, W.A. Friedman, L.W. Woo, V.E. Viola, E.C. Pollacco, C. Volant, and S.J. Yennello, *Phys. Rev. C* **49**, 1516 (1994).
- [14] J. Aichelin and H. Stöcker, *Phys. Lett. B* **176**, 14 (1986);
- J. Aichelin, G. Peilert, A. Bohnet, A. Rosenhauer, H. Stöcker, and W. Greiner, *Phys. Rev. C* **37**, 2451 (1988).

- [15] G. Fáí and J. Randrup, Nucl. Phys. **A404**, 551 (1983).
- [16] W.A. Friedman and W.G. Lynch, Phys. Rev. C **28**, 16 (1983).
- [17] H. Stöcker, G. Buchwald, G. Graebner, P. Subramanian, J.A. Maruhn, W. Greiner, B.V. Jacak, and G.D. Westfall, Nucl. Phys. **A400**, 63c (1983);  
D. Hahn and H. Stöcker, Nucl. Phys. **A476**, 718 (1988);  
D. Hahn and H. Stöcker, Phys. Rev. C **37**, 1048 (1988).
- [18] W.A. Friedman, private communication.

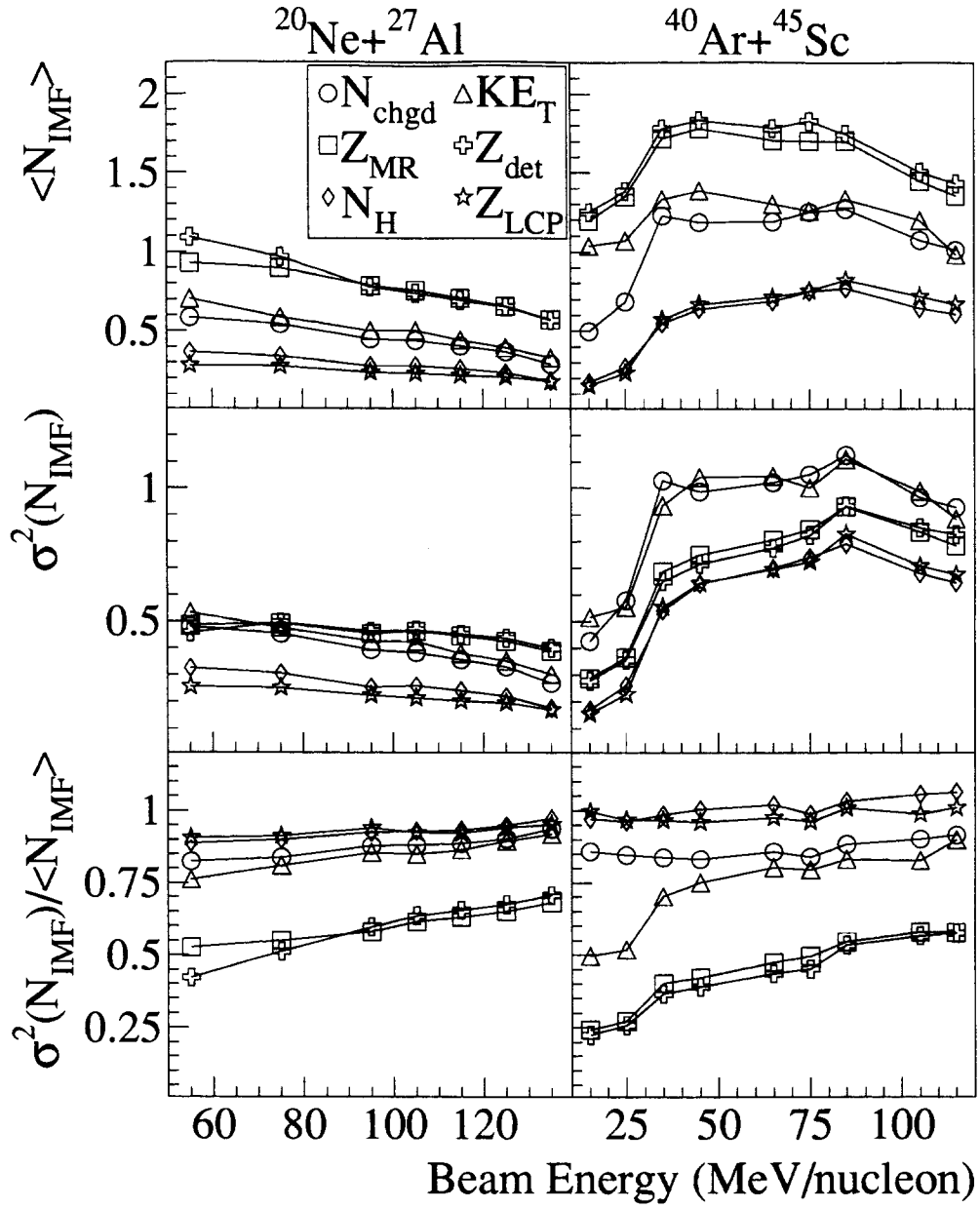


Figure 1: The means, variances, and reduced variances of the IMF multiplicities versus the beam energy in the six separate samples of small impact parameter events for the  $^{20}\text{Ne} + ^{27}\text{Al}$  and  $^{40}\text{Ar} + ^{45}\text{Sc}$  entrance channels.

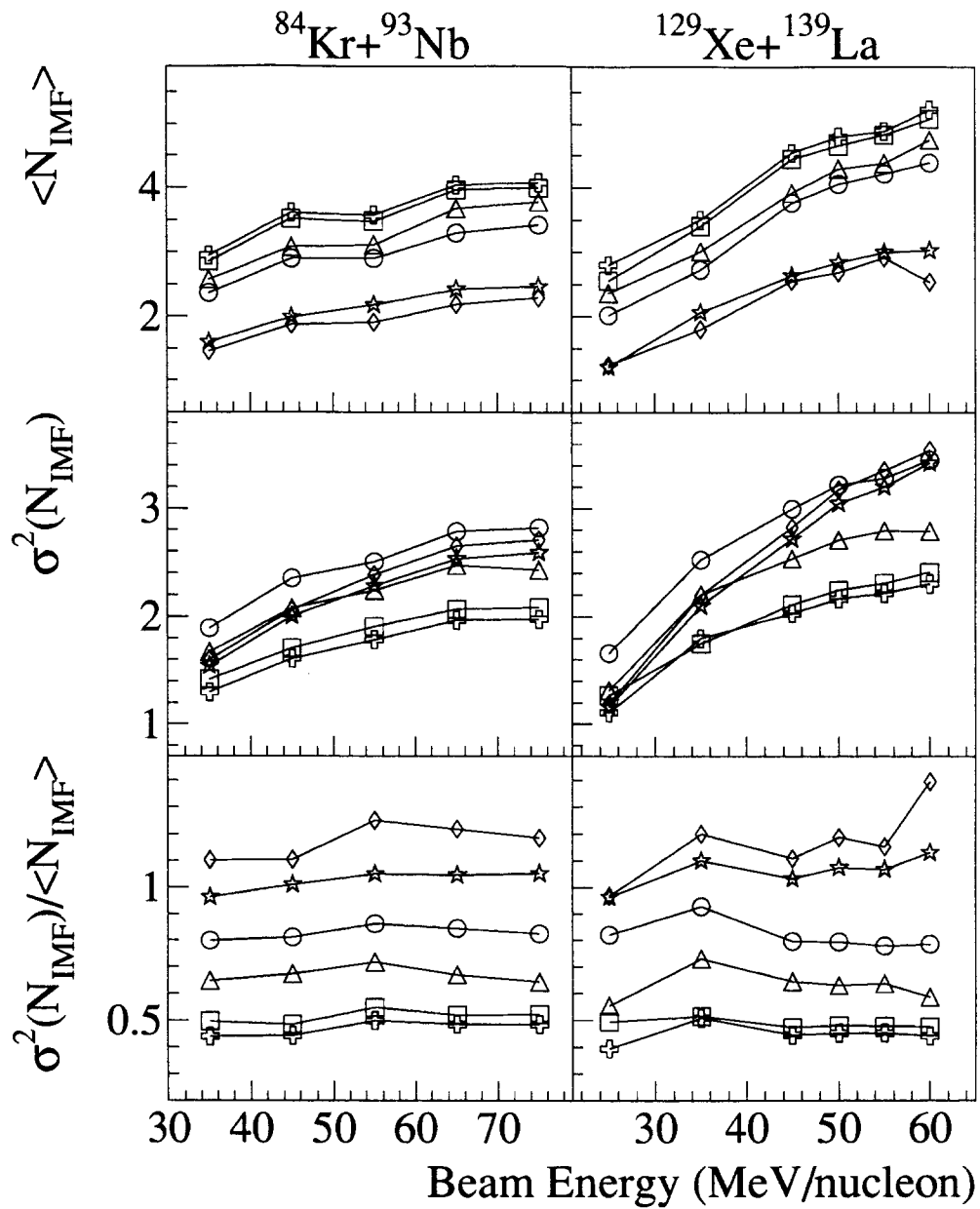


Figure 2: The same as Figure 1, except for the  $^{84}\text{Kr} + ^{93}\text{Nb}$  and  $^{129}\text{Xe} + ^{139}\text{La}$  entrance channels.

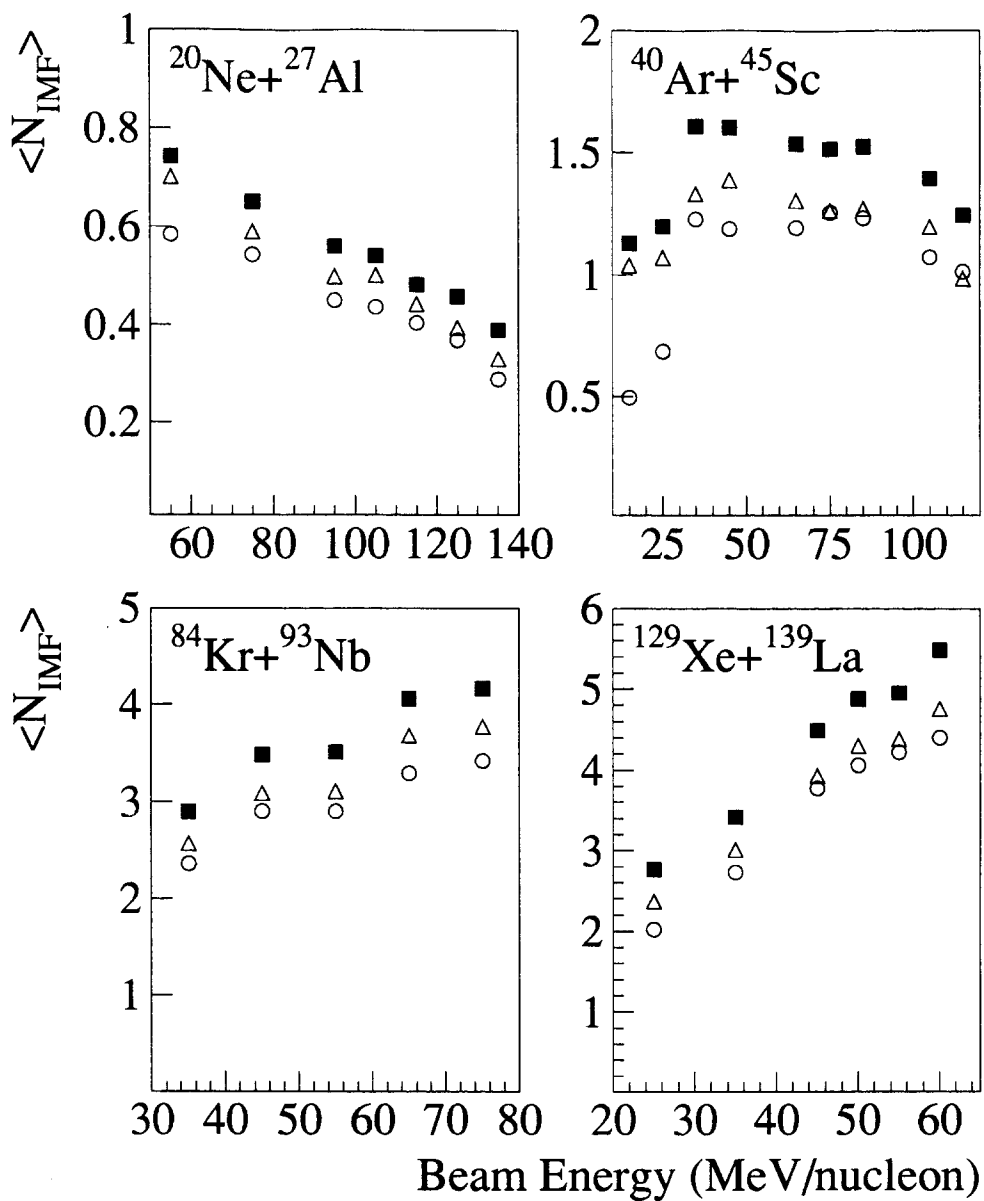


Figure 3: The average number of IMFs versus the beam energy for three samples of small impact parameter events. Shown are the results following the two-dimensional  $\sim 10\%$  cuts on  $N_{chg}$  and  $KE_T$  (solid squares), and following the two one-dimensional  $\sim 10\%$  cuts on  $N_{chg}$  (open circles), and  $KE_T$  (open triangles).



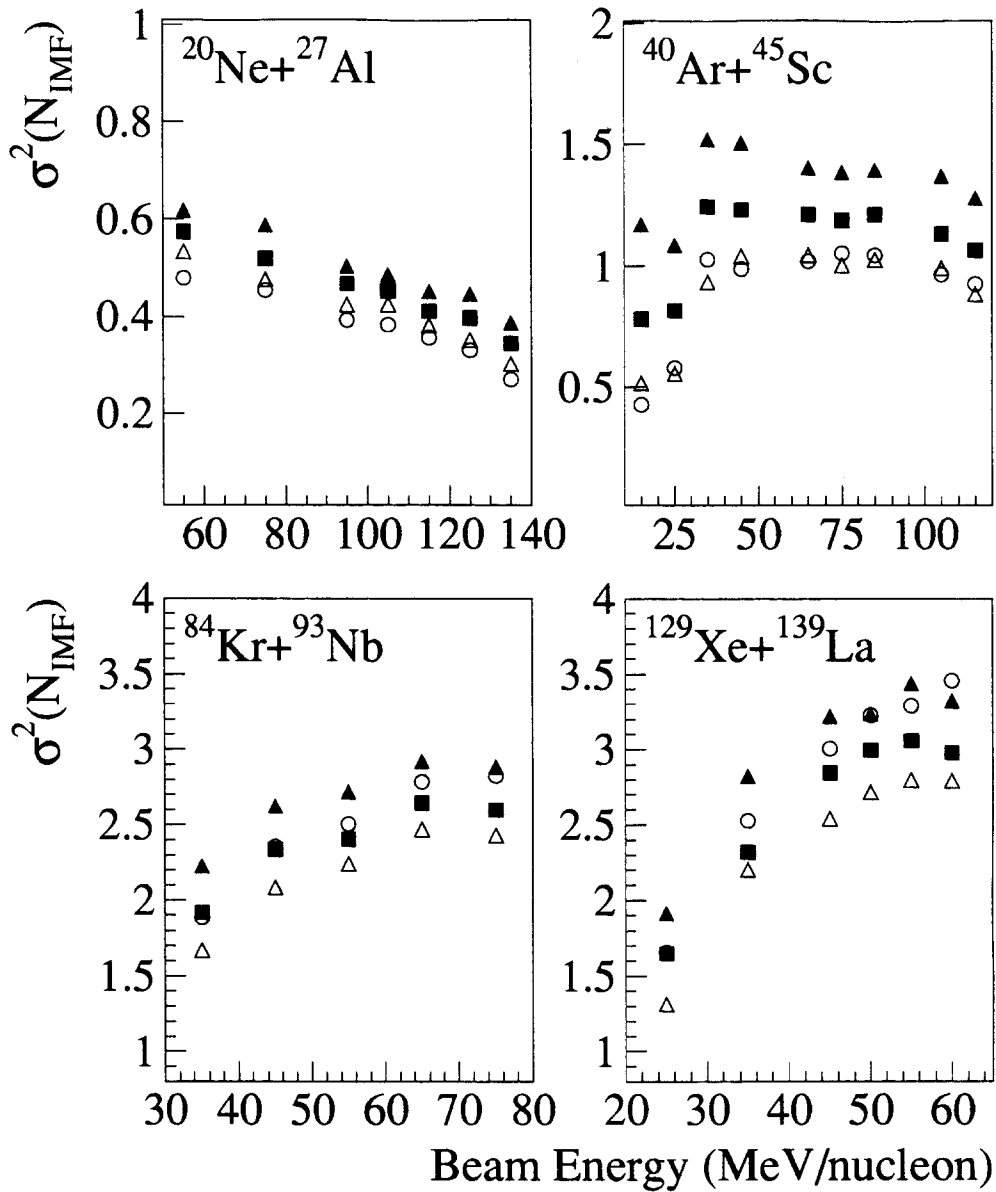


Figure 4: The same as Fig. 3, except for the  $N_{IMF}$  variances in same samples of small impact parameter events. Also shown are these variances following two-dimensional  $\sim 2\%$  cuts on  $N_{chg}$  and  $KE_T$  (solid triangles).

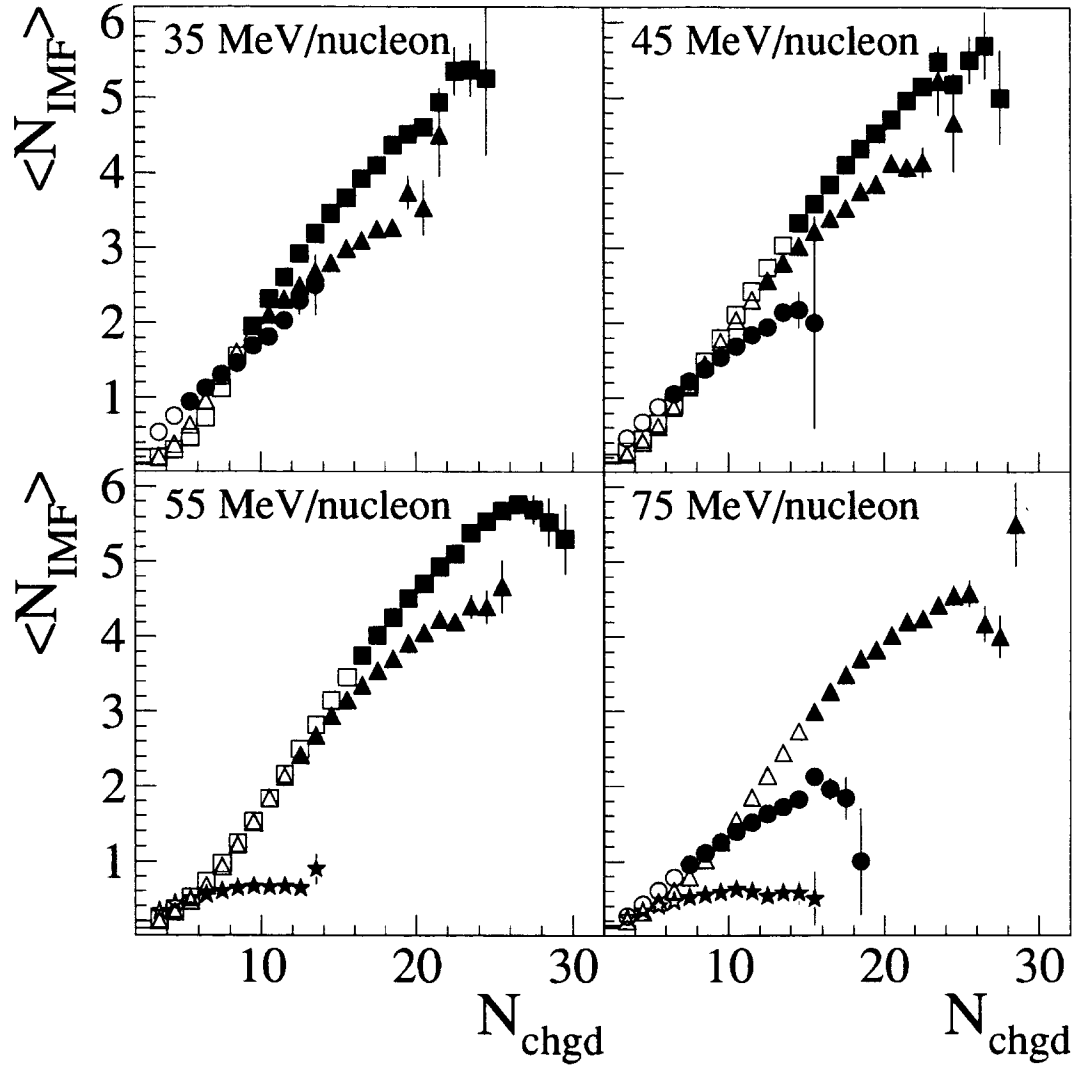


Figure 5: The average number of IMFs versus the total charged particle multiplicity for  $^{20}\text{Ne}+^{27}\text{Al}$  (stars),  $^{40}\text{Ar}+^{45}\text{Sc}$  (circles),  $^{84}\text{Kr}+^{93}\text{Nb}$  (triangles), and  $^{129}\text{Xe}+^{139}\text{La}$  (squares) reactions at four representative beam energies. The values for events above the  $\sim 10\%$  most central thresholds on  $N_{chgd}$  are depicted as the solid points.

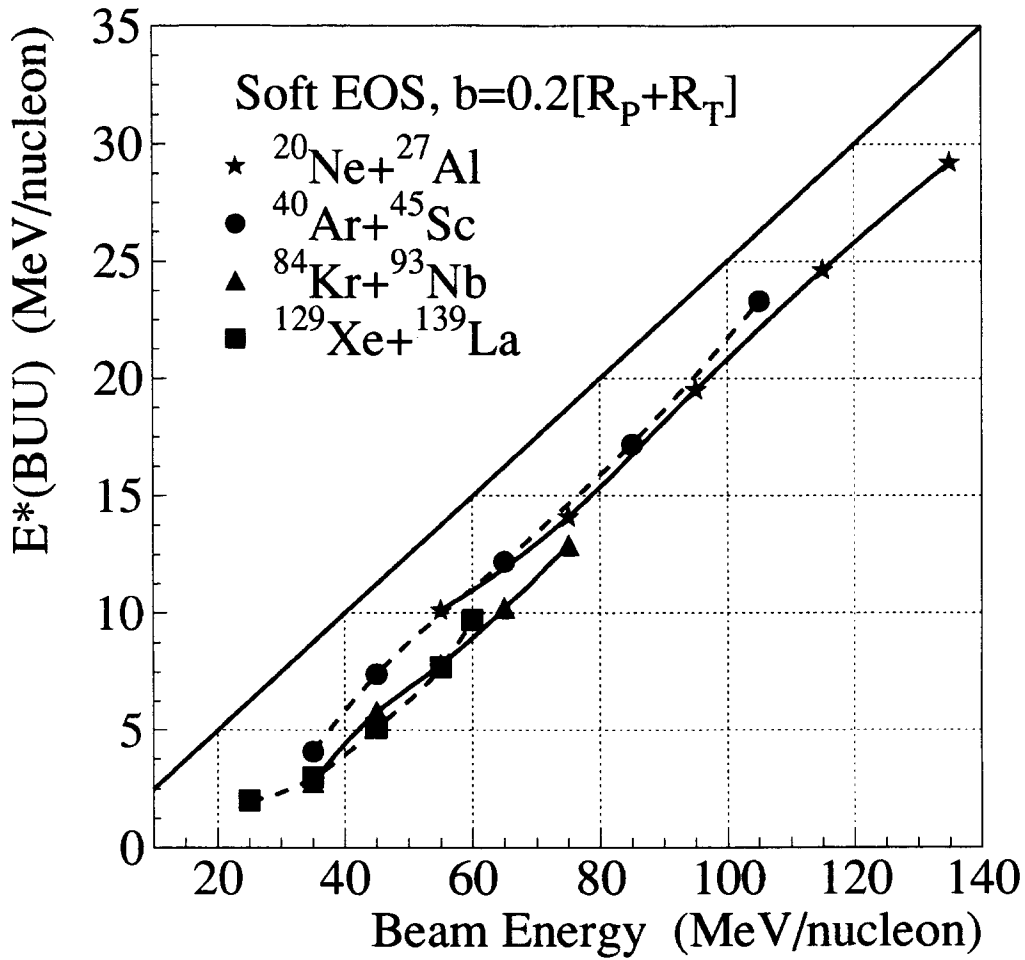


Figure 6: The excitation energies extracted from the BUU calculations for the  $^{20}\text{Ne}+^{27}\text{Al}$  (stars),  $^{40}\text{Ar}+^{45}\text{Sc}$  (circles),  $^{84}\text{Kr}+^{93}\text{Nb}$  (triangles), and  $^{129}\text{Xe}+^{139}\text{La}$  (squares) reactions, assuming an average impact parameter geometrically consistent with the present central event selection and a soft equation of state.

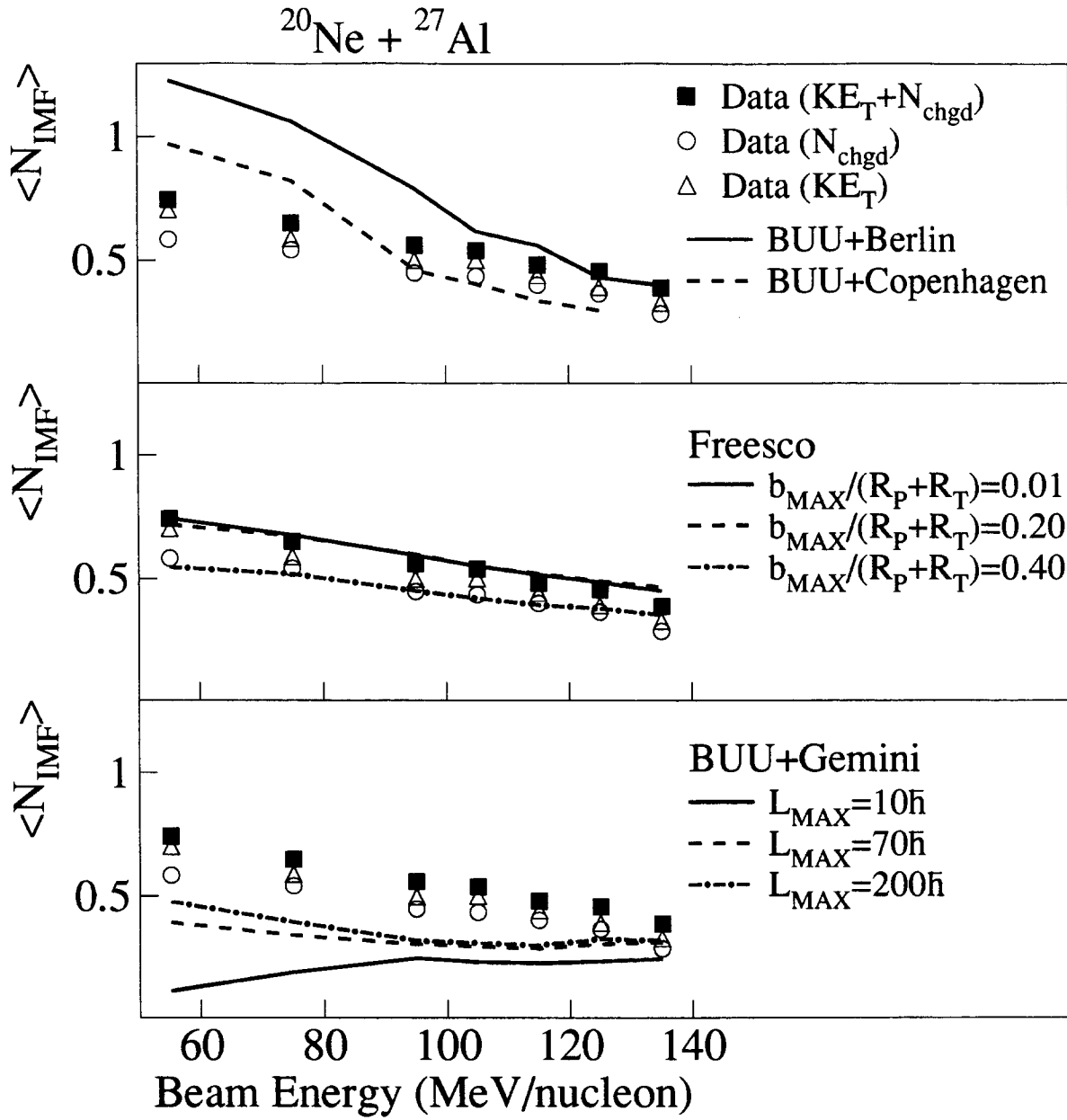


Figure 7: The average IMF multiplicities versus the beam energy in the central  $^{20}\text{Ne} + ^{27}\text{Al}$  reactions. The points are the experimental results for the events selected by the two-dimensional  $\sim 10\%$  cuts on  $N_{\text{chgd}}$  and  $KE_T$  (solid squares), the one-dimensional  $\sim 10\%$   $N_{\text{chgd}}$  cuts (open circles), and by the one-dimensional  $\sim 10\%$   $KE_T$  cuts (open triangles). The lines depict the results from the various filtered model calculations (see text).

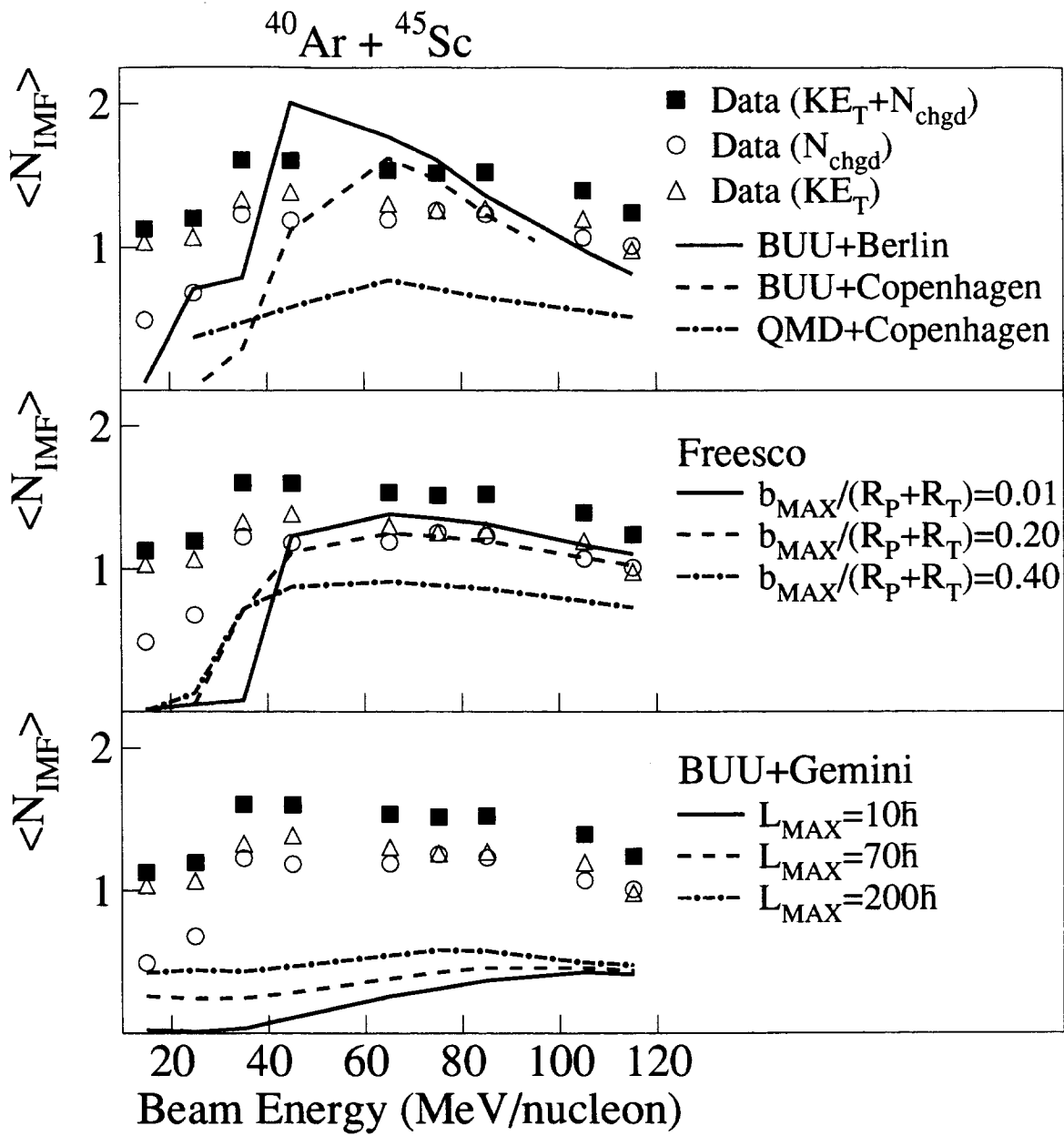


Figure 8: The same as Figure 7, except for the central  $^{40}\text{Ar} + ^{45}\text{Sc}$  reactions.

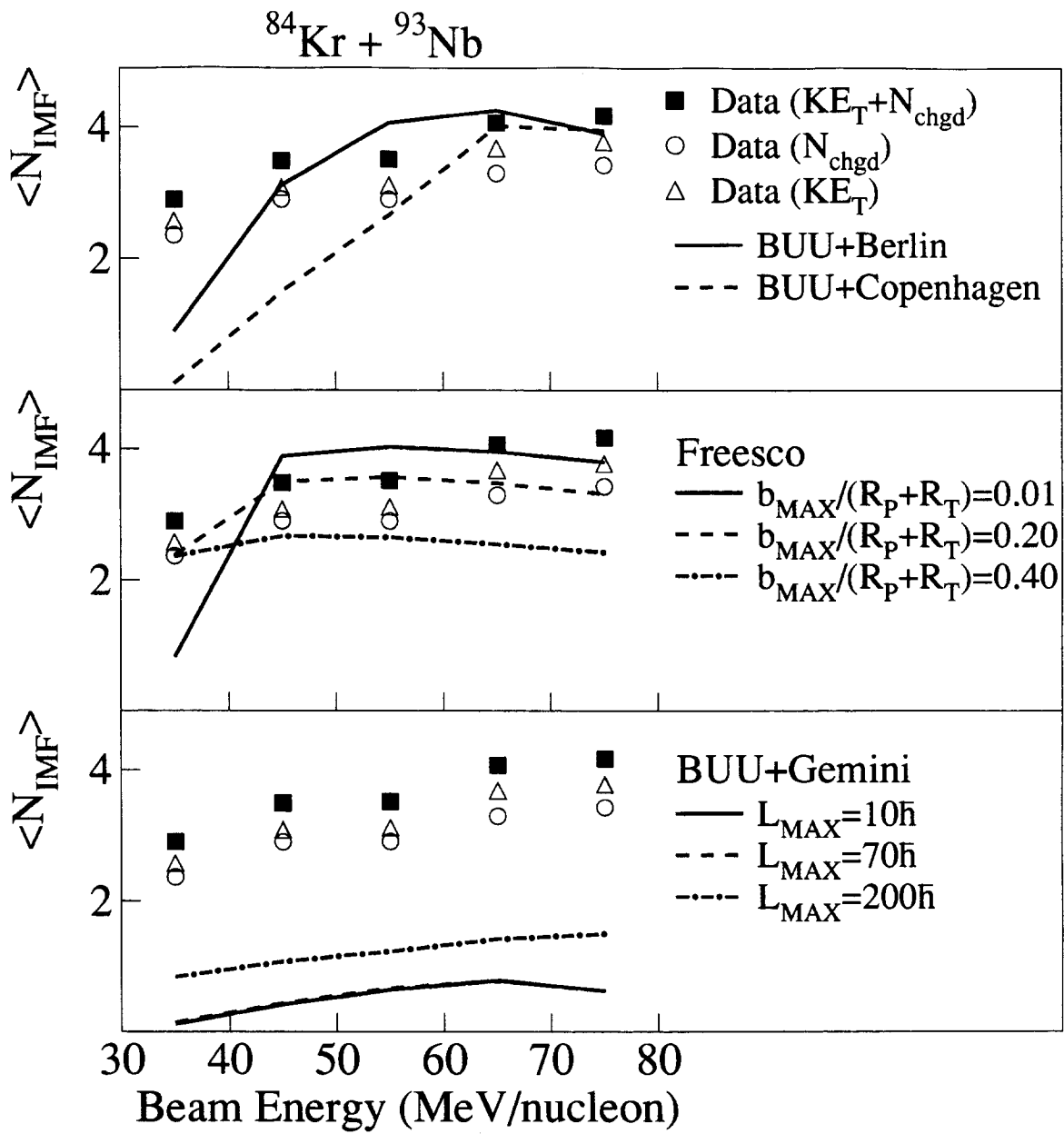


Figure 9: The same as Figure 7, except for the central  $^{84}\text{Kr} + ^{93}\text{Nb}$  reactions.

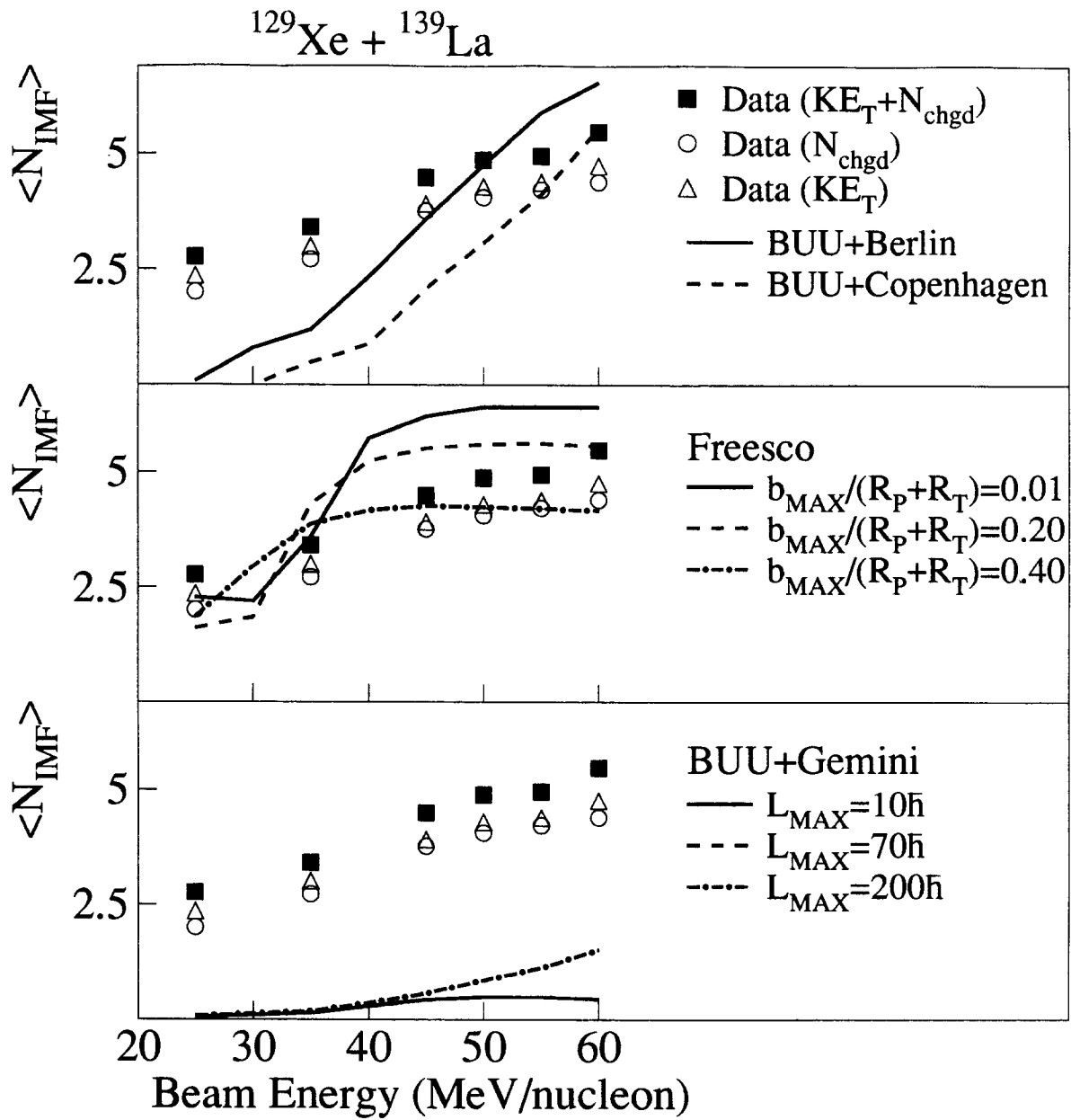


Figure 10: The same as Figure 7, except for the central  $^{129}\text{Xe} + ^{139}\text{La}$  reactions.

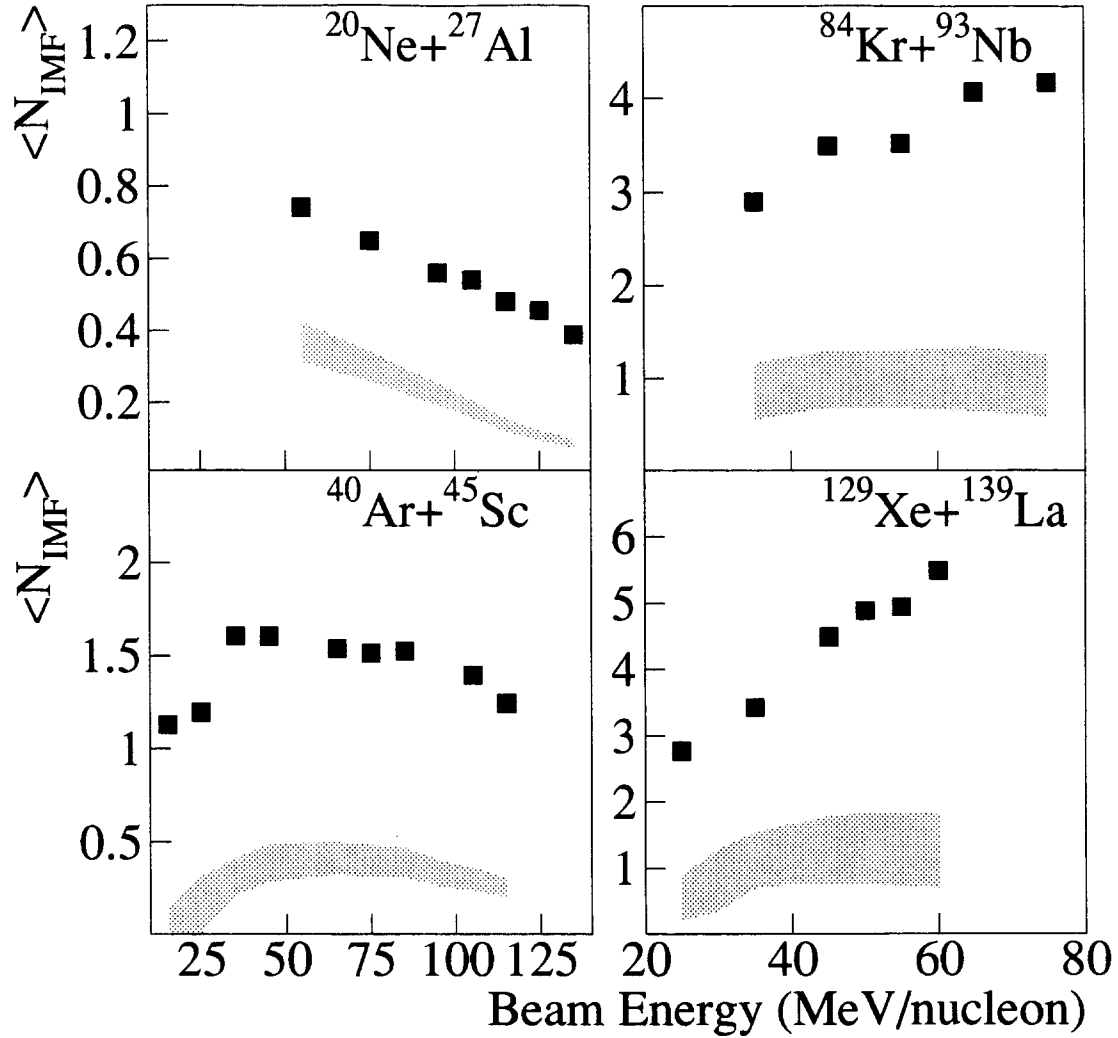


Figure 11: The average IMF multiplicities versus the beam energy for the small impact parameter events selected by the two dimensional  $\sim 10\%$  cuts on  $N_{chgd}$  and  $KE_T$  (solid squares) for all four entrance channels. The shaded regions depict the average IMF multiplicities obtained from the statistical evaporation model of Ref. [16], after an approximate treatment of the experimental acceptance (see text).